Swimming by Reciprocal Motion at Low Reynolds Number

Tian Qiu [1,2], Tung-Chun Lee [1], Andrew G. Mark [1], Konstantin I. Morozov [3], Raphael Münster [4], Otto Mierka [4], Stefan Turek [4], Alexander M. Leshansky [3,5], and Peer Fischer [1,6,*]

[1] Max Planck Institute for Intelligent Systems, 70569 Stuttgart, Germany
[2] Institute of Bioengineering, Ecole Polytechnique Fédérale de Lausanne (EPFL), CH-1015 Lausanne, Switzerland
[3] Faculty of Chemical Engineering, Technion - Israel Institute of Technology, 32000 Haifa, Israel
[4] Institute of Applied Mathematics (LS III), TU Dortmund, Vogelpothsweg 87, 44227 Dortmund, Germany
[5] Technion Autonomous System Program (TASP), 32000 Haifa, Israel
[6] Institut für Physikalische Chemie, Universität Stuttgart, Pfaffenwaldring 55, 70569 Stuttgart, Germany
[*] Corresponding author: P. Fischer, phone: +49-711-689-3560; fax: +49-711-689-3412; E-mail: fischer@is.mpg.de

Abstract

Biological microorganisms swim with flagella and cilia that execute non-reciprocal motions for low Reynolds number (*Re*) propulsion in viscous fluids. This symmetry requirement is a consequence of Purcell's *scallop theorem*, which complicates the actuation scheme needed by micro-swimmers at low *Re*. However, most biomedically important fluids are non-Newtonian where the *scallop theorem* no longer holds. It should therefore be possible to realize a micro-swimmer that moves with reciprocal periodic body-shape changes in non-Newtonian fluids. Here, we report a symmetric "micro-scallop", a single-hinge micro-swimmer that can propel in shear thickening and shear thinning fluids by reciprocal motion at low *Re*. Excellent agreement between our measurements and both numerical and analytical theoretical predictions indicates that the net propulsion is caused by modulation of the fluid viscosity upon varying the shear rate. This reciprocal swimming mechanism opens new possibilities in designing biomedical micro-devices that can propel by a simple actuation scheme in non-Newtonian biological fluids.

Introduction

Motility is important for the survival of many organisms. At the length scale of primitive life-forms, such as bacteria and other microorganisms, locomotion presents a different set of challenges compared to those encountered by macroscopic organisms. Most microorganisms live in fluid environments where they experience a viscous force that is many orders of magnitude stronger than inertial forces. This is known as the low Reynolds number (*Re*) regime

(*Re*<<*1*) characterized by instantaneous and time-reversible flows that are described by the time-independent Stokes equation. A consequence of this is the "scallop theorem", stated by Purcell in his 1976 paper on "Life at low Reynolds number".[1] If a low-Reynolds number swimmer executes geometrically reciprocal motion, that is a sequence of shape changes that are identical when reversed, then the net displacement of the swimmer must be zero, if the fluid is incompressible and Newtonian.[2] In Purcell's own words, "Fast, or slow, it exactly retraces its trajectory, and it's back where it started".[1]

Locomotion at low *Re* therefore generally requires non-reciprocal actuation of the swimmer. In nature, microorganisms break time-reversal symmetry with rotating helices [3] and cilia that show flexible oar-like beats [4]. Inspired by nature, similar swimming strategies have been utilized to propel artificial micro-swimmers. These include helically-shaped micro-propellers that use rigid chiral structures to break symmetry under non-reciprocal unidirectional rotation [5, 6, 7, 8, 9, 10]. As a helix rotates about its long axis, the coupling between rotational and translational motion leads to propulsion at low *Re*. A few flexible micro-swimmers have also been experimentally demonstrated, including a micro-swimmer that is based on a chain of superparamagnetic beads and actuated by a magnet [11], a biohybrid elastic micro-swimmer made of elastic filament and actuated by cardiomyocytes [12], as well as macro-scale model swimmers that use flexible tails [13, 14, 15, 16]. However, in order to break reciprocity, these swimmers require relatively complex fabrication processes and/or actuation mechanisms.

Propulsion of artificial micro-swimmers has mainly been demonstrated in Newtonian fluids, while low *Re* propulsion in non-Newtonian fluids remains relatively unexplored, [17] even though most biological fluids are non-Newtonian. In fact, most of the fluids in the human body are non-Newtonian viscoelastic media, [18] *e.g.* sputum, mucus, and vitreous humor, with many of them, *e.g.* saliva, blood, and synovial fluid, showing shear thinning behavior [19]. Since the scallop theorem no longer holds in complex non-Newtonian fluids, it follows that it should be possible to design and build novel micro-swimmers that specifically operate in these complex fluids.

Fluid elasticity can either enhance [16, 20, 21] or retard [22] propulsion in non-Newtonian fluids. Recent theoretical works on a beating flagellum in a nonlinear viscoelastic Oldroyd-B fluid [23] as well as on a reciprocal sliding sphere swimmer in a shear thinning fluid [24] also suggest that propulsion is achievable by reciprocal motion in which backward and forward strokes occur at different rates. Similarly, the elasticity of the fluid has enabled low *Re*

propulsion of oscillating asymmetric dimers. [25] However, low *Re* locomotion of a true reciprocal motion micro-swimmer propelled by periodic body-shape changes has not been reported previously.

Here, we build and actuate single-hinge micro- and macro-swimmers that move in the manner of the "scallop" described by Purcell.[1] The dimensions of the micro-scallop are sub-millimeter, approaching the size regime of relevance for non-invasive exploration of, for instance, blood vessels. Even though they are restricted to reciprocal motion, the scallops achieve low *Re* propulsion by using a time-asymmetric stroke pattern, and exploiting the strain rate dependent viscosity of shear thickening and shear thinning fluids. Precise control over the macro-scallop permits quantitative comparison with our numerical modelling results and analytical theory for the propulsion mechanism. Excellent agreement between experiment and theory is found, confirming that the net propulsion is caused by the differential apparent fluid viscosity under asymmetric shearing conditions. The results demonstrate that, despite the scallop theorem, in biologically relevant fluids simple actuation schemes can generate propulsion.

Results

Design and actuation of the micro-scallop

Our micro-scallops are constructed from PDMS, loaded with phosphorescent pigment, cast into a 3-D printed mold, which permits the use of different materials in a parallel fabrication process. Each micro-scallop consists of two thick (300 μm) shells connected by a thin (60 μm), narrow (200 μm) hinge (Fig 1(B)). Rare earth micro-magnets (Ø200 μm × 400 μm) are attached to each shell so that when exposed to an external magnetic field the two magnets reorient to align with the field and each other and thus close the micro-scallop (Fig 2(A) right). When the magnetic field is decreased, the restoring force of the PDMS hinge provides the recovery stroke, opening the micro-scallop (Fig 2(A) left). The thick stiff shells and compliant flexible hinge ensure that the deformation is isolated at the hinge. As stated by Purcell: any single-hinge structure can only exhibit reciprocal motion.[1]

The opening angle α of the micro-scallop is related to the strength of the applied external field. As shown in Fig 2(C), asymmetric actuation of the two shells is achieved by applying a periodic exponentially decaying current to generate the magnetic field. Typically a 0.5 Hz waveform was used with a slow ~1.9 s exponential decay, followed by a rapid 0.1 s ramp. Since a gradient-free field is used, the micro-magnets do not experience any pulling force,

which ensures the net displacement of the micro-swimmer is due to the propulsion caused by its own shape-changing swimming motions.

Propulsion of the micro-scallop in a shear thickening fluid

Forward net displacement of the micro-scallop in a shear thickening fluid (fumed silica in Poly(propylene glycol)) was achieved by time-asymmetric actuation of the opening angle as seen in Fig 3(A). Overlaying five frames with the same opening angles α taken at 50 s intervals (Fig 3(A)), clearly shows net displacement in the x direction parallel to the magnetic field direction (movie S1 upper panel). As a control, the micro-scallop in the same fluid was actuated with a symmetric wave-form, and, as expected, no net displacement in the x-direction was observed (Fig 3(B) and movie S1 lower panel). Furthermore, asymmetric actuation in a Newtonian fluid (glycerol) also yields no net displacement (circles in Fig 3(C)).

Fumed silica particle suspensions were chosen as the shear thickening fluid, because of their well-known characteristics [26] and relatively high viscosity. The dynamic viscosity of the fluid is in the range of $1-22$ Pa·s (Fig 4(A)), and its density is 1051 ± 2 kg/m^3. The micro-scallop swam for more than 100 μm over 10 periods, and the average velocity was 5.2 μm/s (3.5% body length/cycle). If we take the characteristic maximum length of the micro-scallop as 1 mm, and the largest forward velocity as 3 mm/s, then the calculated *Re* $=1.4\times10^{-4}-3\times10^{-3}\ll1$. Thus, the micro-swimmer operates at a very low *Re* [1] using only reciprocal motion.

Propulsion of the micro-scallop in a shear thinning fluid

Propulsion of the micro-scallop operated with a reciprocal but asymmetric actuation sequence is also achieved in hyaluronic acid, a shear thinning solution found in a number of biological systems. In the shear thinning fluid the micro-scallop only moves forward when the opening-closing cycle is opposite to that of the shear thickening fluid. Now, fast-opening followed by a slow-closing step gives forward propulsion. About 65 μm displacement was covered by the micro-scallop in 10 periods, corresponding to an average velocity of 3.8 μm/s (2.5% body length/cycle). As in the shear thickening medium, the micro-scallop showed no significant forward displacement when the opening and closing cycles were symmetric, as is expected (see movie S2).

Analytical theory of propulsion by reciprocal motion in the shear thickening fluid

We consider a simple model of a flapping, Purcell scallop-like swimmer with the typical spatial dimension l composed of two counter-rotating shells that share a common axis. For simplicity we assume that the shells open and close with different angular speeds, $\omega_{slow} = \omega$ and $\omega_{fast} = p\omega$, where ω_{slow} and ω_{fast} stand for the velocity of the slow and fast stroke, respectively, so that $p \geq 1$ for all swimming gaits. The maximum rotation angle of one plate is $\alpha/2$ and the scallop completes one full cycle in period $T = \frac{\alpha}{2\omega} + \frac{\alpha}{2p\omega} = \frac{\alpha(p+1)}{2p\omega}$. Thus, the net force exerted by the tethered swimmer (*i.e.* pump) on the fluid can be estimated (up to an arbitrary function of the opening angle α) as

$$F_p \sim \frac{1}{T}\left(-\int_0^{\alpha/2\omega} \mu_{app}\, \omega l^2 dt \; + \; \int_{\alpha/2\omega}^{\alpha(p+1)/2p\omega} \mu_{app}\, p\omega l^2 dt\right) \quad (1)$$

where μ_{app} is an apparent (spatially averaged) viscosity of the fluid, which depends on the instantaneous shear rate, and the history of the flow.

Note that for a Newtonian fluid, the net force over one cycle in equation (1) is zero, as expected from the "scallop theorem", *i.e.* no net momentum can be transferred to a fluid by a pump using geometrically reciprocal strokes [1]. However, for a non-Newtonian fluid, the dependence of the apparent viscosity on the shear rate breaks time-reversibility and from equation (1) the net force over a period is

$$F_p \sim \frac{1}{T}\left[-\bar{\mu}_{app}^{slow}\, \omega l^2 \left(\frac{\alpha}{\omega}\right) + \bar{\mu}_{app}^{fast}\, p\omega l^2 \left(\frac{\alpha}{p\omega}\right)\right] = \frac{\omega l^2 p}{p+1} \Delta\bar{\mu}_{app} \quad (2)$$

where $\bar{\mu}_{app}^{slow}$, $\bar{\mu}_{app}^{fast}$ are the apparent viscosities time-averaged over respectively slow and fast strokes with $\Delta\bar{\mu}_{app}$ being their difference.

The propulsion velocity of the *force-free swimmer* V_s can be estimated from $F_p = F_d$, where F_d is the force to be applied to an inactive swimmer in order to drag it with velocity V_s. This is in accord with the duality relation between pushing and swimming, *i.e.* $-\boldsymbol{V}_s \cdot \boldsymbol{F}_p = P_d$, where P_d is the power (rate-of-work) invested to drag the inactive swimmer [27]. Since $P_d = -\boldsymbol{V}_s \cdot \boldsymbol{F}_p$, the relation $F_p = F_d$ follows. Assuming that $F_d \sim \mu_0 V_s l$, where μ_0 is the apparent viscosity corresponding to the typical shear rate magnitude V_s/l. For low values of the shear rate associated with swimming, *i.e.* $V_s/l << \omega$, it is reasonable to assume that $\mu_0 \approx const$ (the rheological measurements (Fig 4(A)) suggests that for shear rates up to 1.7 s^{-1} viscosity is roughly constant).

Equating F_d and F_p in equation (2) yields the propulsion velocity up to an unknown function of angle α:

$$\frac{V_s}{\omega l} \sim \frac{p}{p+1} \frac{\Delta \bar{\mu}_{app}}{\mu_0} \quad (3)$$

More detailed analysis of a flapping swimmer composed of two infinite plates (see SI) suggests that the major contribution to $\Delta \bar{\mu}_{app}$ in Equation (3) is due to an abrupt rise (fall) of apparent viscosity of the shear thickening (shear thinning) fluid sandwiched between two close plates at *small* openings during the *fast* phase (either closing or opening, see SI for details).

To model propulsion through shear thickening fluid, a power law equation [28] was applied to fit the transition-region of the viscosity in the shear rate range of 1.5 - 6 s^{-1} (dotted line in Fig 4(A)). The apparent viscosity is $\bar{\mu}_{app} = m\dot{\gamma}^{n-1}$, where m, n are constants ($m = 0.34, n = 3.34$ as fitted in this case) and $\dot{\gamma}$ is the shear rate defined as $\dot{\gamma} = \left(2D_{ij}D_{ij}\right)^{\frac{1}{2}}$ *i.e.* the second invariant of the rate-of-strain tensor $D_{ij} = \frac{1}{2}(\partial_i u_j + \partial_j u_i)$. Obviously, in this problem the typical shear rate is, respectively, $\dot{\gamma} \sim \omega$ for opening and $\dot{\gamma} \sim p\omega$ for closing. Thus, assuming that both (*i.e.* fast and slow) strokes fall within the shear thickening regime, $\bar{\mu}_{app}^{slow} \sim m\omega^{n-1}$ and $\bar{\mu}_{app}^{fast} \sim m(p\omega)^{n-1}$, Equation (3) becomes

$$\frac{V_s}{\omega l} \sim \left(\frac{\bar{\mu}_{app}^{slow}}{\mu_0}\right) \frac{(p^{n-1}-1)p}{p+1} \quad (4)$$

Multiplying V_s in Equation (4) by the stroke period $T = \frac{\alpha(p+1)}{p\omega}$ we obtain a simple expression for the scaled displacement-per-stroke, D/l,

$$D/l \sim \beta(p^{n-1} - 1) \quad (5)$$

where the sign and magnitude of the dimensionless pre-factor β depends on the nature of the stroke and fluid properties. The analytical theory therefore clearly confirms that in a shear thickening fluid, the scallop can indeed swim forward using fast closing and slow opening strokes. Alternatively, it can propel in the opposite direction using fast opening and slow closing strokes. This is a general result that permits propulsion from symmetric actuation in any of the abundant non-Newtonain fluids, notably those found in biological systems. In order to allow for quantitative comparisons between the predictions of this analytical theory and experiment, we now consider a millimeter-scale low *Re* scallop-like swimmer whose motion is controlled by on-board motors. The device, which

we call the "macro-scallop" (shown in Fig 1(C) and Fig S5, S6), permits rapid and precisely controlled opening and closing speeds of the swimmer's shells.

Tests of the analytical theory were conducted in shear thickening fluid in two regimes: i) fixed opening speed ω_o over a range of closing speeds $\omega_c > \omega_o$ (Fig 4(B)) and ii) fixed closing speed ω_c at different opening speeds $\omega_o > \omega_c$ (Fig 4(C)). When the closing speeds are larger than the opening speed ($p = \frac{\omega_c}{\omega_o}$), the net displacement D/l is larger than 0 and the macro-scallop moves in the forward direction (hinge leading). On the other hand, when the opening speeds (hollow triangles) are larger than the closing velocities (solid squares, $p = \frac{\omega_o}{\omega_c}$), the swimmer moves in the opposite direction with a negative net displacement $D/l < 0$ (hinge trailing). Both experimental results are in excellent agreement with the theory of equation (5) based on scaling arguments. It follows that a symmetric scallop can indeed move, provided time-reversal symmetry is broken by the asymmetric actuation speeds of opening and closing in a non-Newtonian fluid. Note that the two actuation gaits (*i.e.* fast opening/slow closing *vs.* fast closing/slow opening) resulted in a different displacement for the same value of p due to viscosity hysteresis (see SI).

Numerical model of propulsion by reciprocal motion in the shear thickening fluid

We have also employed numerical simulations to study the propulsion mechanism of reciprocal motion in non-Newtonian fluids using the open-source Computational Fluid Dynamics (CFD) package FeatFlow (detailed method in the SI). Figure 5(A) and Movie S4 show the fluid velocity and viscosity fields at 6 frames through the complete 4 s propulsion cycle of the macro-scallop swimming in a shear thickening fluid. The net displacement in one cycle is clear from the difference in swimmer position between the start (0 s) and finish (4 s) of the cycle. The propulsion mechanism is illustrated by comparing the field maps at 0.3 s and 2.4 s; these frames both correspond to the same $\alpha = 115^{\circ}$, however the higher closing angular velocity of the shells leads to a much higher velocity gradient (shear rate) of the fluid at 0.3 s, which results in larger viscosity between the two shells relative to that during the opening stroke (at 2.4 s). Therefore, the forward displacement during the fast closing half-cycle (upper panels in Fig 5(A)) is larger than the backward displacement in the slow opening half-cycle (lower panel in Fig 5(A)), which leads to the net displacement over one period. The displacement curves (Fig 5(B)) of the simulation show excellent quantitative agreement with the experimental data in both the Newtonian and shear thickening cases. The simulation results demonstrate that the net propulsion is a result of the viscosity differences during the two half-cycles, which is caused

by differential apparent fluid viscosity under asymmetric shearing conditions. Importantly, consistent results were achieved using only the simple shear thickening relationship between fluid viscosity and instantaneous shear rate. This suggests that the dominant factor leading to net propulsion in our experiment is differential viscosity rather than fluid energy storage mechanisms like fluid elasticity or viscosity hysteresis (thixotropy/rheopecty).

Discussion

We have shown that low-*Re* propulsion of a scallop is possible in shear thickening and shear thinning fluids. The devices are true swimmers, propelled by periodic body-shape changes.[17] Differences in the opening and closing rates give rise to differences in the corresponding shear rates and hence the viscosities of the non-Newtonian fluid. The result is net propulsion despite the reciprocal stroke. Unlike reference [25], fluid elasticity plays only a minor role; rheological measurements (Fig S7, S8) show that the first normal stress difference of our shear thickening medium is two orders of magnitude smaller than the Boger fluid used in [25]. Furthermore the numerical simulations, which do not include elasticity effects, accurately reproduce the motion, and experiments with a time symmetric stroke ($p = 1$) produce no net propulsion. In summary, our swimmer fulfills three conditions necessary for propulsion by reciprocal motion at low *Re* in the absence of elasticity: 1) absence of mirror symmetry in the direction of motion (*i.e.* a clear fore-aft asymmetry) 2) time-asymmetric actuation and 3) the coupling of such an actuation to a non-Newtonian fluid rheology. Because the time asymmetry of the stroke is responsible for the net displacement, the direction of propulsion can be reversed by inverting the opening and closing speeds. This is a potential benefit over other micro propulsion schemes where the direction of motion is dictated by the fixed spatial asymmetry of the device [16, 25].

We found that the average velocity of the micro-scallop in the shear thickening fluid is faster than that in the shear thinning one, because for the same difference in shear rates the change in fluid viscosity is larger in the shear thickening fluid. This is apparent from the differences in the n exponents in the power law models. The swimming velocity can be increased by maximizing the difference in the opening and closing speeds, up to the point where the viscosity plateaus at ~7 s^{-1}. Optimizing the shape of the swimmer can also be expected to improve performance. The viscosity is highly dependent on the shear rate, which is not only determined by the speed of opening and closing, but is also a function of the swimmer shape. Optimizing the geometric shape of the swimmer (and the morphology of its surfaces) may thus have a significant effect on propulsion speed of a non-Newtonian micro-swimmer.

A simple theory that relies on scaling arguments has been derived that captures the essential underlying physical mechanism of the locomotion, *i.e.* via shear rate modulation of the viscosity. The highest shear rate is achieved when the fluid is sandwiched between the two shells at *small* openings during the *fast* stroke phase and the corresponding abrupt change of the apparent viscosity controls the net displacement over a stroke. The weakly thixotropic property of the shear thickening fluid also plays a minor role in the propulsion. In our case the viscosity hysteresis provides a speed advantage to those gaits where the $\omega_o > \omega_c$ versus those where $\omega_c > \omega_o$. In principle, large viscosity hysteresis could be used to generate net displacement even for time-symmetric strokes.

Micro-swimmers have the potential to be useful in biomedical applications or as rheological probes *in vivo*. Swimming in biological fluids is a first step to achieve these goals. Halyoronic acid is found in connective, epithelial, and neural tissues [29]; and it is one of the main components of the extracellular matrix, which contributes significantly to cell proliferation and migration [30]. Many biological media including saliva, blood, vitreous and synovial fluid exhibit shear thinning properties, and as we show here this can be exploited in the design and operation of a micro-swimmer that is simpler to operate than many other microrobots. From an engineering point of view, reciprocal motion can be achieved with much simpler actuation schemes compared to non-reciprocal actuators. Most existing (miniaturized) actuators are reciprocal, including piezoelectric, bimetal stripes, shape memory alloy, heat or light actuated polymers, which can all potentially be used as actuators for the micro-swimmer demonstrated here. Thus, the reciprocal swimming mechanism of the micro-scallop reported in this paper may provide a general scheme for micro-swimming in biological fluids.

Methods

3-D printing and molding process for the micro-scallop

The negative mold of the micro-scallop (shown in Fig S1) was printed with a high temperature material (RGD 525) using a 3-D printer (Objet260 Connex, Stratasys, Israel). The support-material was removed by magnetic stirring in KOH solution (0.03 g/ml) for 12 hours. 2 g of Ultra Green V10 Glow powder (2-8 micron, Glow Inc., MD) was mixed with 15 ml ethanol by sonication for 1 hour, and the supernatant was collected and dried under vacuum. 2 g base agent of Polydimethylsiloxane (PDMS, Sylgard® 184, Dow Corning) was added to the dried Glow powder,

mixed thoroughly under sonication for 1 hour. 100 µl curing agent was then added, and the solution was thoroughly mixed and degassed for 1 hour. The 3-D printed mold was filled with the prepared PDMS solution and degassed for 0.5 h and cured at 65 °C for 1.5 h. Finally, the PDMS shell was released from the mold and two Neodymium micro-magnets ($\varnothing 0.2\ \text{mm} \times 0.4\ \text{mm}$, GMB Magnete Bitterfeld GmbH, Germany) were stuck to the shells using Cyanoacrylate (Ultra Gel, Pattex) under a stereoscope with the help of an external macro-magnet as illustrated in Fig S3.

Preparation of the fluids and rheological measurements

Fumed silica suspensions (8% w/w) were used as the shear thickening fluid.[26] Fumed silica powder (Aerosil® 150, Evonik, Germany) was mixed thoroughly with poly(propylene glycol) (PPG, M_w=725, Sigma-Aldrich). The solution was then degassed for 3 h.

Hyaluronic acid (6 mg/ml) was used as the shear thinning fluid. Hyaluronic acid powder (53747, Sigma-aldrich) was mixed in PBS (Gibco®, Life Technologies) and stirred under room temperature for 48 hours.

Glycerol (99.5%, 1410 mPa·s at 20 °C, VWR, France) and Silicone oil (Dow Corning 200/12,500 cSt, VWR, UK) were used as Newtonian fluids for micro-scallop and macro-scallop, respectively.

The viscosities were measured using shear rate ramp experiments on a rheometer (Kinexus Pro, Malven, UK) using a plate to plate (40 mm in diameter) setup. The temperature was set to 25 °C. The viscosity was measured in the range of 0.05-300 s^{-1} with a 4 min ramp time. The data shown in Fig 5 and S9 are the average of three independent measurements of two fluids, respectively.

Actuation setup and video analysis of the micro-scallop

The micro-scallop was actuated by an external magnetic field, generated by a Helmholtz coil which can produce homogeneous magnetic fields of up to approximately 300 G in the swimming direction of the micro-scallop (indicated by the red arrow in Fig 2(A)). Detail about the setup is drawn in Fig S4 and discussed in the SI.

Videos of the micro-scallop were taken under a stereoscope (MZ95, Leica, Germany) with a CCD camera (DFC490, Leica, Germany) at 20 frames/s, with UV illumination by a LED (peak wavelength at 365 nm, Roithner Laser Technik GmbH, Germany) and a colored-glass filter (485-565 nm, VG9, Schott, Germany). Every frame of the

video was extracted using ffmpeg and the sequential images were analyzed by customized Matlab script to extract the coordinates of the mid-point of the hinge and the angle between the two shells in every frame. The frames, in which the angle α reaches its minimum value of 40°, are selected from each period and are used to deduce the displacement. Five selected frames between 0-200 s with interval of 50 s were overlapped in Fig 3(A) and 3(B) using ImageJ (NIH), and for comparison the micro-scallop was aligned at the same y-axis position. Each experiment was repeated five times.

Numerical simulation and analytical analysis

The numerical simulations were conducted using the CFD package FeatFlow (www.featflow.de) as a solver for the incompressible Navier-Stokes equations. A quasi 2D approach was used in such way that the thickness of the computational domain was set to a small value. The rheological properties of the non-Newtonian fluid were modeled by a piecewise continuous approximation to the measured viscosity profile (Fig S12). The simulations were conducted over three complete opening/closing cycles. The simulation volume was 45 mm × 90 mm × 1 mm, using 60000 timesteps with dt=0.0002 s. Meshes were generated by a grid-adaptation technique that concentrates vertices at the fluid-solid interface. The methods for the numerical simulation and analytical analysis are discussed in more details in the SI.

Acknowledgements

The research was in part supported by the European Research Council under the ERC Grant agreement Chiral MicroBots (278213), by the Rubin Scientific and Medical Research Fund (A.M.L.), by the Israel Ministry for Immigrant Absorption (K.I.M.), and by the Deutsche Forschungsgemeinschaft (DFG) as part of the project DFG (NV): TU 102/43-1. The authors thank Ms. U. Heinrichs for help with the rheology measurement and Ms. I. Nuss and Dr. H. Boehm for the preparation of the HA solutions. The simulations were conducted on the LiDOng cluster of the TU Dortmund. The authors thank the LiDOng cluster administration for their support and assistance.

Author contributions

T.Q., T.-C.L., A.G.M., P.F. designed the experiments. T.Q. performed the experiments. T.Q., T.-C.L., A.G.M. analyzed the data. K.I.M., A.M.L. performed analytical theory study. R.M., O.M, and S.T. performed numerical

simulations. P.F. conceived the project and supervised the experiments. All authors contributed to the writing of the paper.

Competing financial interests: The authors declare no competing financial interests.

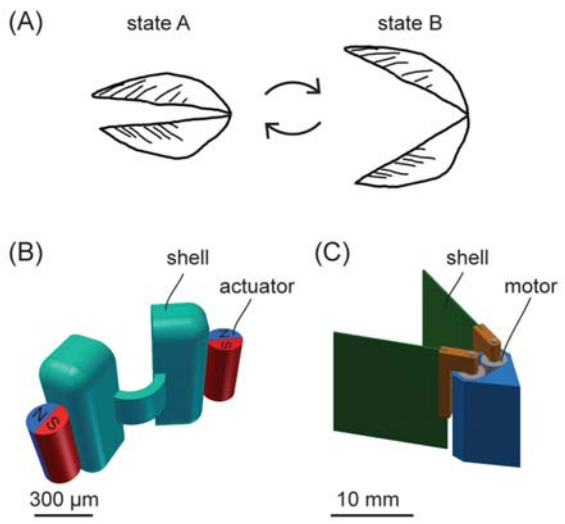

Fig 1. Schematic drawing of the scallop swimmers. (A) Schematic drawing of Purcell's scallop with reciprocal motion.[1] (B) 3-D model of the sub-millimeter size "micro-scallop". (C) 3-D model of the centimeter size "macro-scallop" for quantitative comparison with theory.

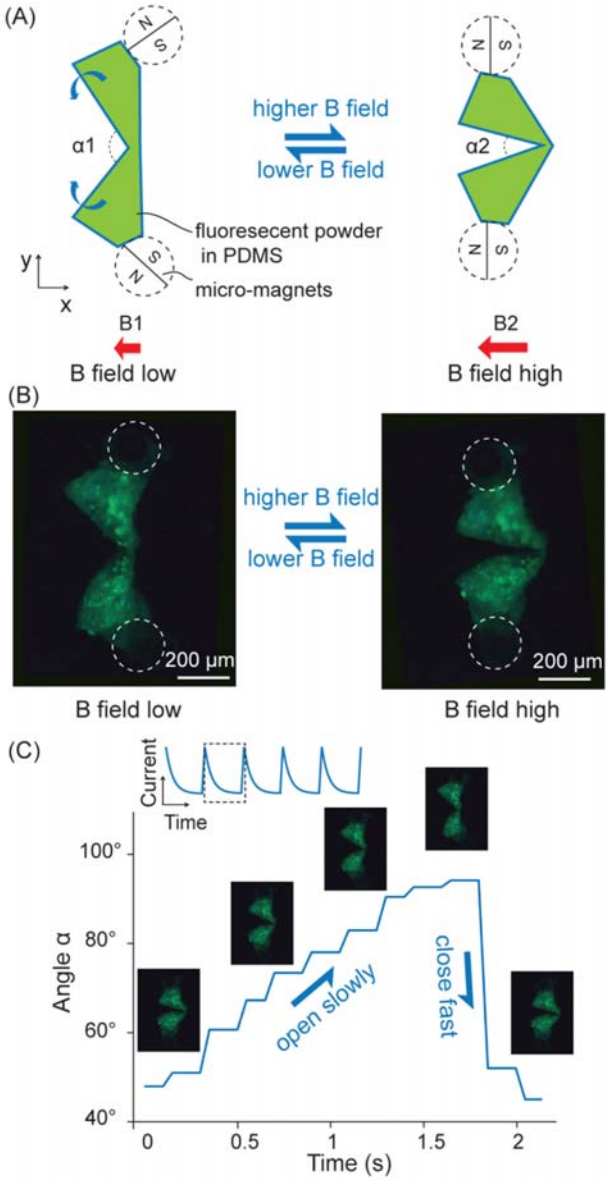

Fig 2. Actuation mechanism of the micro-scallop. (A) Schematic drawing of the micro-scallop from top view. The green shapes illustrate the opening and closing shape change of the micro-scallop when actuated by an external magnetic field. The shape is a function of the magnetic force aligning the magnetic axes of the two permanent micro-magnets and a restoring force due to the induced stress in the PDMS structure. The angle between the two shells α can therefore be controlled by the magnitude of the external field. (B) Top view (microscope image) of the micro-scallop under UV illumination. The positions of the micro-magnets are illustrated by white dashed circles. (C) Time-asymmetric actuation of the micro-scallop. The slow opening and the fast closing cycles are controlled by the external magnetic field, which is generated by an exponentially decaying current (inset). Corresponding images of the micro-scallop during the opening and closing cycle are shown.

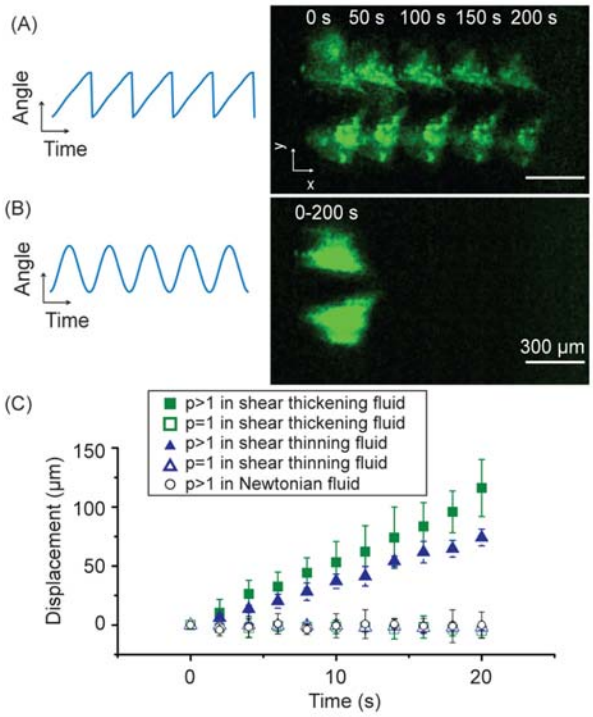

Fig 3. Displacement of the micro-scallop in a shear thickening and a shear thinning fluid. (A) Forward net displacement of the micro-scallop in a shear thickening fluid and asymmetric actuation (blue curve). The image is a time lapse composite-picture of 5 frames at an interval of 50 s, with the net displacement indicated along the x direction (see movie S1 upper panel). (B) Corresponding image of the micro-scallop in shear thickening fluid with symmetric actuation (blue curve) and no discernable net displacement (see movie S1 lower panel). (C) Corresponding displacement curves in the shear thickening, shear thinning and Newtonian fluids respectively. ω_c and ω_o are the average angular velocity of closing and opening, respectively. Asymmetric actuations ($p = \omega_{fast}/\omega_{slow} = \omega_c/\omega_o > 1$ solid squares and $p = \omega_{fast}/\omega_{slow} = \omega_o/\omega_c > 1$ solid triangles) result in net displacement in non-Newtonian fluids, while symmetric actuations ($p = \omega_{fast}/\omega_{slow} = 1$, hollow squares and triangles) result in no net displacement in the same fluids (see Movie S2 for swimming in shear thinning fluid). Asymmetric actuations ($p = \omega_{fast}/\omega_{slow} = \omega_c/\omega_o > 1$, circles) result in no net displacement in the Newtonian fluid (see Movie S3), as stated by the scallop theorem. The error bars correspond to the standard deviation of repeated trials.

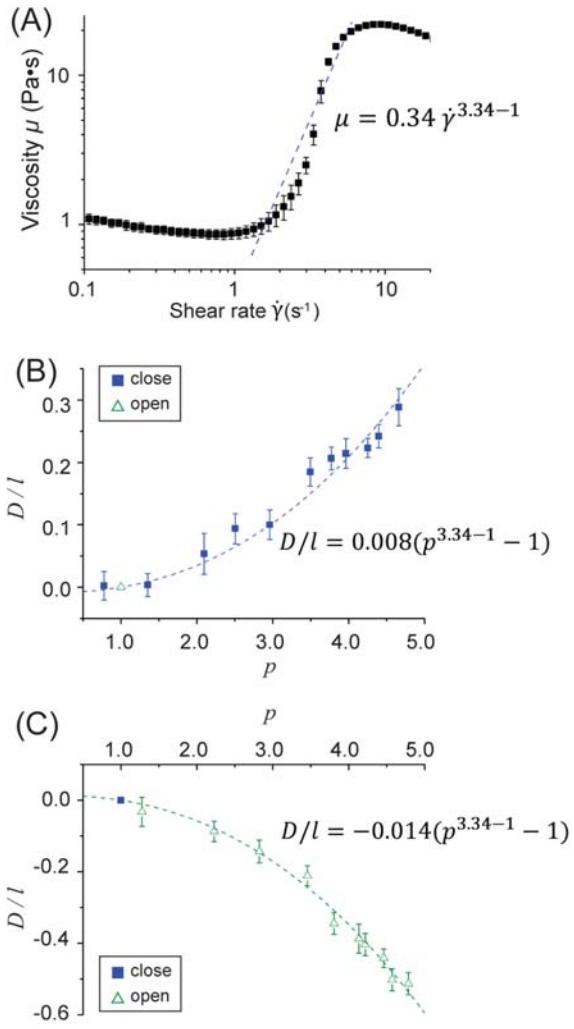

Fig 4. Comparison between theoretical predictions and experimental measurements of scallop swimming. (A) Apparent dynamic viscosity of the shear thickening fluid. The dotted line shows the power law used to fit the transition of the experimental shear thickening data (solid squares). (B) Dimensionless net displacement over one period is plotted against the ratio of angular velocities. When the closing velocities (solid squares) are larger than the opening velocity (hollow triangle), $p = \omega_{fast}/\omega_{slow} = \omega_c/\omega_o > 1$, the swimmer exhibits positive net displacements, as predicted the scaling theory. (C) When the opening velocities (hollow triangles) are larger than the closing velocity (solid square), $p = \omega_{fast}/\omega_{slow} = \omega_o/\omega_c > 1$, the swimmer exhibits negative net displacements. In (B) and (C), D and l are the displacement over one stroke and characteristic length, respectively. The error bars correspond to the standard deviations.

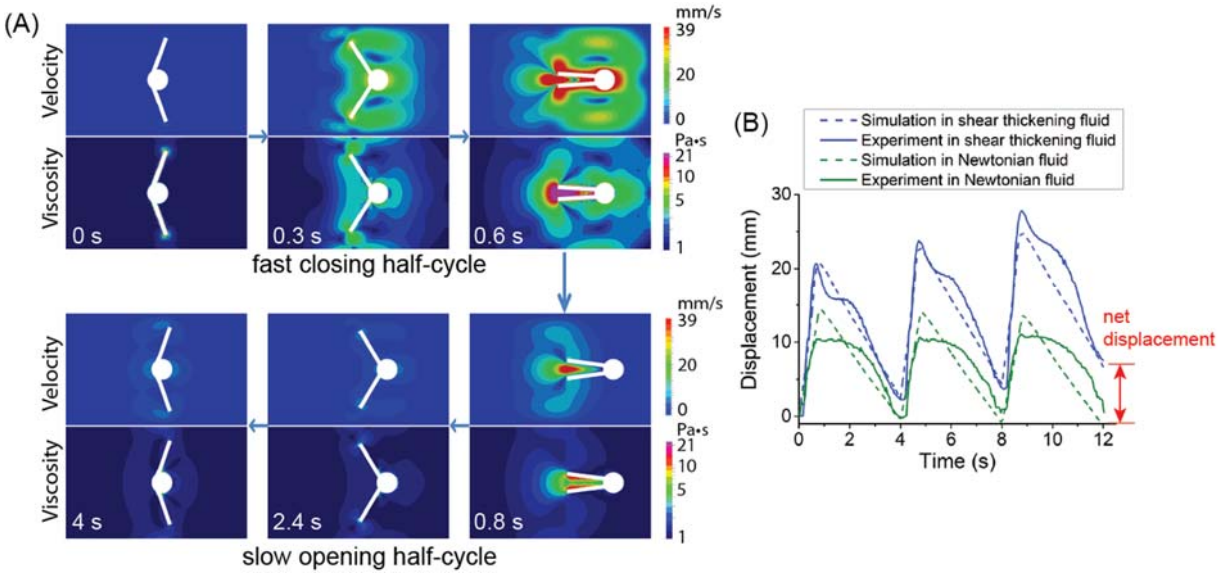

Fig 5. Numerical simulation of propulsion by reciprocal motion in a shear thickening fluid. (A) Fluid velocity and viscosity fields around the swimmer in shear thickening fluid (see also Movie S4). The three images in the upper panel correspond to the fast closing half-cycle (~0.8 s) and the images in the lower panel correspond to the slow opening half-cycle (~3.2 s). The simulation result verifies that the net displacement is a result of the viscosity differences during the two half-cycles, which is caused by the differences in fluid shear rate (velocity gradient) under asymmetric actuation. (B) The displacement curves of the asymmetric actuated macro-scallop in shear thickening (blue) and Newtonian fluid (green) for 3 cycles. Simulation results (dashed lines) are consistent with experimental data (solid lines), where the macro-scallop exhibits net displacement in the shear thickening fluid but no net displacement in the Newtonian fluid.

References

1. Purcell EM. Life at Low Reynolds-Number. *Am J Phys* **45**, 3-11 (1977).
2. Lauga E. Life around the scallop theorem. *Soft Matter* **7**, 3060-3065 (2011).
3. Turner L, Ryu WS, Berg HC. Real-time imaging of fluorescent flagellar filaments. *J Bacteriol* **182**, 2793-2801 (2000).
4. Brokaw CJ. Non-Sinusoidal Bending Waves of Sperm Flagella. *J Exp Biol* **43**, 155-169 (1965).
5. Ghosh A, Fischer P. Controlled Propulsion of Artificial Magnetic Nanostructured Propellers. *Nano Lett* **9**, 2243-2245 (2009).
6. Mark AG, Gibbs JG, Lee TC, Fischer P. Hybrid nanocolloids with programmed three-dimensional shape and material composition. *Nat Mater* **12**, 802-807 (2013).
7. Schamel D, Pfeifer M, Gibbs JG, Miksch B, Mark AG, Fischer P. Chiral Colloidal Molecules And Observation of The Propeller Effect. *J Am Chem Soc* **135**, 12353-12359 (2013).
8. Zhang L, Abbott JJ, Dong LX, Kratochvil BE, Bell D, Nelson BJ. Artificial bacterial flagella: Fabrication and magnetic control. *Appl Phys Lett* **94**, 064107 (2009).
9. Tottori S, Zhang L, Qiu FM, Krawczyk KK, Franco-Obregon A, Nelson BJ. Magnetic Helical Micromachines: Fabrication, Controlled Swimming, and Cargo Transport. *Adv Mater* **24**, 811-816 (2012).
10. Li J, *et al.* Template electrosynthesis of tailored-made helical nanoswimmers. *Nanoscale*, DOI: 10.1039/C3NR04760A (2014).
11. Dreyfus R, Baudry J, Roper ML, Fermigier M, Stone HA, Bibette J. Microscopic artificial swimmers. *Nature* **437**, 862-865 (2005).
12. Williams BJ, Anand SV, Rajagopalan J, Saif MTA. A self-propelled biohybrid swimmer at low Reynolds number. *Nat Commun* **5**, 3081 (2014).
13. Sudo S, Segawa S, Honda T. Magnetic swimming mechanism in a viscous liquid. *J Intel Mat Syst Str* **17**, 729-736 (2006).
14. Guo SX, Pan QX, Khamesee MB. Development of a novel type of microrobot for biomedical application. *Microsyst Technol* **14**, 307-314 (2008).
15. Pak OS, Gao W, Wang J, Lauga E. High-speed propulsion of flexible nanowire motors: Theory and experiments. *Soft Matter* **7**, 8169-8181 (2011).
16. Espinosa-Garcia J, Lauga E, Zenit R. Fluid elasticity increases the locomotion of flexible swimmers. *Phys Fluids* **25**, 031701 (2013).
17. Lauga E, Powers TR. The hydrodynamics of swimming microorganisms. *Reports on Progress in Physics* **72**, 096601 (2009).
18. Fung YC. Bio-viscoelastic Fluids. In: *Biomechanics* (Fung YC). Springer (1981).
19. Cone RA. Mucosal Immunology. In: *Mucosal Immunology* (Mestecky J, Lamm ME, Strober W, Bienenstock J, McGhee JR, Mayer LW). Academic (2005).
20. Teran J, Fauci L, Shelley M. Viscoelastic fluid response can increase the speed and efficiency of a free swimmer. *Physical review letters* **104**, 038101 (2010).
21. Liu B, Powers TR, Breuer KS. Force-free swimming of a model helical flagellum in viscoelastic fluids. *P Natl Acad Sci USA* **108**, 19516-19520 (2011).
22. Lauga E. Propulsion in a viscoelastic fluid. *Phys Fluids* **19**, 083104 (2007).
23. Fu HC, Wolgemuth CW, Powers TR. Swimming speeds of filaments in nonlinearly viscoelastic fluids. *Phys Fluids* **21**, 033102 (2009).
24. Montenegro-Johnson TD, Smith DJ, Loghin D. Physics of rheologically enhanced propulsion: Different strokes in generalized Stokes. *Phys Fluids* **25**, 081903 (2013).
25. Keim NC, Garcia M, Arratia PE. Fluid elasticity can enable propulsion at low Reynolds number. *Phys Fluids* **24**, 081703 (2012).
26. Raghavan SR, Khan SA. Shear-thickening response of fumed silica suspensions under steady and oscillatory shear. *J Colloid Interf Sci* **185**, 57-67 (1997).
27. Raz O, Avron JE. Swimming, pumping and gliding at low Reynolds numbers. *New J Phys* **9**, 437 (2007).
28. Barnes HA. Shear-Thickening (Dilatancy) in Suspensions of Nonaggregating Solid Particles Dispersed in Newtonian Liquids. *J Rheol* **33**, 329-366 (1989).
29. Laurent TC, Laurent UB, Fraser JR. The structure and function of hyaluronan: An overview. *Immunology and cell biology* **74**, A1-7 (1996).

30. Trochon V, *et al.* Evidence of involvement of CD44 in endothelial cell proliferation, migration and angiogenesis in vitro. *International journal of cancer Journal international du cancer* **66**, 664-668 (1996).

Supplementary Information

Design and fabrication process of the micro-scallop

The micro-scallop was readily realized by 3-D printing and micro-molding technique, shown in Fig S1. Fig S2 shows the detailed dimensions of the micro-scallop. The hinge is both narrow (200 μm) and thin (60 μm) to decrease the elastic force against the magnetic force, while the two shells are much thicker (300 μm) to avoid any deformation during the actuation. This ensures the motion is reciprocal, as stated by Purcell that any single-hinge structure can only result in a reciprocal motion. The shells (800 μm) are also wider than the hinge (200 μm), which enables larger contact area with the fluid and results in better propulsion.

After the PDMS part was released from the mold, two Neodymium micro-magnets (Ø0.2 mm×0.4 mm, GMB Magnete Bitterfeld GmbH, Germany) were attached to the shells by glue (Ultra Gel, Pattex) in two steps. As illustrated in Fig S3(A), one macro-magnet was first used on the left side and the micro-magnet on the left was glued to the PDMS at the right orientation under the stereoscope. After the fixation of the first micro-magnet, the macro-magnet was moved to the right, and the second micro-magnet on the right was glued to the PDMS (Fig S3(B)). During the second step, the local field dominated by the field of the macro-magnet, so the orientation of the second micro-magnet was kept in the opposite direction of the first one.

Actuation setup of the micro-scallop

Because the micro-magnets have much higher density (~7400 kg/m^3) than the fluids (~1000 kg/m^3), it will sink to the bottom in an upright 5 mm-height container within 30 s and then the friction between the micro-scallop and the bottom will severely affect the propulsion of the micro-scallop. Therefore, the fluidic channel was placed in a reversed manner to minimize the friction and the micro-scallop was held on the interface of fluid and air by interfacial force while the micro-scallop was immersed in the fluid, as illustrated in Fig S4. The width and height of the fluidic channel are 5 mm and 3 mm, which are about 8 and 4 times of the corresponding size of the micro-scallop to minimize the boundary effect of swimming at low *Re*. The Helmholtz coil (yellow rings in Fig S4) provided a homogeneous magnetic field up to 300 G.

Macro-scallop design and experimental setup

Fig S5 is the 3-D model of the macro-scallop model swimmer. It was designed to be the smallest size as possible for a low *Re* using commercially available motors. Two brushless DC-motors (0308H with a 03A gear head, total size 3.4 mm in diameter and 12.6 mm in length, Faulhaber, Germany) were used and the speed and the rotational direction are controlled by a controller (SC1801F, Faulhaber, Germany) with analog input 0.5 V- 12 V to set speed value. One full period of the macro-scallop was set to 4 s, with about 0.8 s for fast closing half-cycle and 3.2 s for slow opening half-cycle (Fig 5(A) and Fig S6(B)).

The shells are made of carbon fiber sheet (0.3 mm thick, Conrad, Germany). Two sizes were used for the experiment, *i.e.*16 mm ×14 mm (Length×Width) for the illustration of swimming and compare to numerical simulation result; and 8 mm ×7 mm (Length×Width) to test the theory of the scaling argument. Small area of the shell decreases the power needed for rotation in very viscous fluid, thus the motors can provide higher rotating velocity and achieve higher ratio p of closing and opening angular velocities.

As illustrated in Fig S6(A), a linear air track (Edu-lab, UK) was used to balance the gravity of the macro-scallop to make it swim in a force-free situation. For imaging, green phosphorescent tape (Conrad, Germany) was stuck to the bottom of the shells and the body. A UV lamp (peak wavelength at 365 nm) illuminated from the side of the tank and the video was taken by a digital camera at 25 frames/s with a colored-glass filter (485-565 nm, VG9, Schott, Germany). Fig S6(B) is a series of time-lapse pictures showing one cycle of slow-open-fast-close asymmetric actuation of the macro-scallop and the resulted net displacement in shear thickening fluid (also see Movie S4), while there was no net displacement by symmetric actuation in the same fluid (see Movie S5).

Numerical simulation of the macro-scallop

The numerical simulations of the macro-scallop in non-Newtonian and Newtonian fluids were conducted using the open-source CFD (Computational Fluid Dynamics) package FeatFlow (www.featflow.de). We configured the 3D simulation to use a pseudo 2D setup which means that the thickness of the swimmer and the computational domain are reduced. Thus the number of degrees of freedom in the simulation is significantly reduced as is the computational cost. In the following we will briefly explain the numerical methods used to simulate the macro-

scallop swimmers in Newtonian and non-Newtonian fluids. In our FeatFlow software the fluid is modelled by the incompressible Navier-Stokes equations which can be formulated as

$$\begin{cases} \varrho \partial_t \vec{v} + \varrho(\vec{v} \cdot \nabla)\vec{v} + \nabla p = \nabla \cdot \mathbb{S} + f \\ \nabla \cdot \vec{v} = 0 \end{cases} \quad (1)$$

$$\mathbb{S} = \mu(\nabla \vec{v} + \nabla \vec{v}^T) \quad (2)$$

where we denote the constant density by ρ, the shear dependent viscosity by μ, the unknown velocity and pressure by the pair $(\vec{v}, p)$, and the viscous stress tensor by $\mathbb{S}_{ij} = 2\mu D_{ij}$, in which D_{ij} is the rate-of-strain tensor.

This system of equations is discretized using the Finite Element Method (FEM) which is implemented in our FeatFlow CFD package together with the recent extensions of non-Newtonian fluids and dynamic mesh-adaptation for moving boundaries.

Discretization in time is handled by the basic one-step Θ-scheme (3), which in general allows the selection of Crank-Nicolson ($\Theta = 0.5$) or the fully implicit Backward Euler-Scheme ($\Theta = 1$). The time discretization scheme in general can be represented by the following system:

For given $\vec{v}^{n-1}, p^{n-1}$ and $\Delta t = t_n - t_{n-1}$, lets approximate $\partial_t \vec{v}|_{t_n} \approx \frac{\vec{v}^n - \vec{v}^{n-1}}{\Delta t}$

$$\begin{cases} \varrho\left(\vec{v}^n - \vec{v}^{n-1}\right) + \Delta t \Theta\left((\vec{v}^n \cdot \nabla)\vec{v}^n + \nabla \cdot \left(\mu(\nabla \vec{v}^n + (\nabla \vec{v}^n)^T)\right)\right) + \Delta t \nabla p^n = \\ \qquad = \Delta t(\Theta - 1)\left((\vec{v}^{n-1} \cdot \nabla)\vec{v}^{n-1} + \nabla \cdot \left(\mu(\nabla \vec{v}^{n-1} + (\nabla \vec{v}^{n-1})^T)\right)\right) \\ \nabla \cdot \vec{v}^n = 0 \end{cases} \quad (3)$$

The system is then discretized in space using the Galerkin variational formulation of the Navier-Stokes equations. In our FEM framework we use the higher order Q_2/P_1 element pair for the spatial discretization, further aspects of the FEM approach are described in more detail in our previous work [1]. Concerning the physical properties of the fluid, the density ρ is assumed to be constant, wheareas the viscosity μ is calculated at each cubature point according to the given shear-dependent rheological model. The system needs additional adjustment because of the presence of moving boundaries (the macro-scallop). These are treated by the so-called Fictitious Boundary Method (FBM) [1] which is a simple filter technique that decomposes the computational domain into a fluid and a solid subdomain in terms of the classification of the degrees of freedom. The fluid domain is then treated as if no FBM were applied, the solid subdomain interacts with the fluid subdomain by the imposed velocity Dirichlet boundary conditions (*i.e.* the

rotational and translational velocity of the macro-scallop). The velocity of the macro-scallop is calculated by determining the hydrodynamic forces [1] that arise from the movement of the scallop. In order to improve the accuracy of the hydrodynamic force calculation we employ a grid-adaptation technique that is based on Laplacian smoothing using weights that force the vertices of the mesh to be concentrated at the fluid-solid interface (Fig S11).

Test of the theory by scaling argument

The macro-scallop with shells of 8 mm ×7 mm (Length×Width) were used to test the theory of the scaling argument. The closing half-cycle and the opening half-cycle were tested separately at various angular velocities. The largest opening angle $\alpha = 295^{\circ}$ and the smallest closing angle $\alpha = 10^{\circ}$ were kept the same among all the tests by mechanical limit. Each closing and opening velocity was repeated for at least three times.

The time of shell closing or opening and the resulted displacements were calculated from the recorded video. Every frame of the video was extracted by ffmpeg. The first frame in which the swimmer moved was labeled as the start frame. The last frame in which the swimmer stopped moving was labeled as the end frame. In the start and end frame, the frame number N_1 and N_2, x and y coordinates of the body tip (x_1, y_1) and (x_2, y_2), were measured in ImageJ (NIH) respectively, so that the following parameters were calculated:

Time of the half-cycle, $t = \frac{N_2 - N_1}{f}$, where f = 25 frames/s is the frame rate;

Average angular velocity, $\omega = \frac{295^{\circ} - 10^{\circ}}{t} = \frac{285^{\circ}}{t}$;

Displacement over half-cycle, $D = \sqrt{(x_2 - x_1)^2 + (y_2 - y_1)^2}$ for the forward displacement in the closing half-cycle, and $D = -\sqrt{(x_2 - x_1)^2 + (y_2 - y_1)^2}$ for the backward displacement in the opening half-cycle.

The scaled displacement-per-stroke, D/l were calculated, where the characteristic length of the micro-scallop $l = 7\ mm$, and it is plotted against the ratio p of average angular velocities in Fig 4(B) and 4(C) to compare with the theory by scaling argument.

Modulation of viscosity as underlying mechanism of propulsion

Let us consider an idealized tethered "scallop" (pump) composed of two infinite plates forming an angle α between them. The plates are co-rotating on a common axis with an arbitrary angular velocity ω. For simplicity we assume that the suspending medium is a Newtonian fluid. It is possible, however, to extend this solution and construct the asymptotic expansion corresponding to weakly non-Newtonian fluid (*e.g.* shear thinning or thickening) by the method of perturbations [2], however for our qualitative purposes the leading order solution suffices.

We consider the problem in the polar coordinates (r, φ). The solutions for the streamfunction $\psi(r, \varphi)$ in the Stokes approximation satisfy $\nabla^4\psi = 0$. Following [3] and using an ansatz $\psi = r^2 f(\varphi)$ we find the solution for ψ the 'inner' (in between plates) and 'outer' regions, respectively:

$$\psi^{in}(r, \varphi) = -\frac{\omega r^2}{2}\frac{\sin 2\varphi - 2\varphi\cos 2\alpha}{\sin 2\alpha - 2\alpha\cos 2\alpha} = -\frac{\omega r^2}{2A_{in}}[\sin 2\varphi - 2\varphi\cos 2\alpha], \quad (4)$$

$$\psi^{o}(r, \varphi) = -\frac{\omega r^2}{2}\frac{\sin 2\varphi + 2(\pi - \varphi)\cos 2\alpha}{\sin 2\alpha + 2(\pi - \alpha)\cos 2\alpha} = -\frac{\omega r^2}{2A_{o}}[\sin 2\varphi - 2(\pi - \varphi)\cos 2\alpha], \quad (5)$$

where A_{in} and A_o are the functions of α. The velocity components $v_r = \frac{1}{r}\partial\psi/\partial\varphi$ and $v_\varphi = -\frac{1}{r}\partial\psi/\partial r$ can be readily obtained from the Equations (4-5); for the inner region we have:

$$v_r^{in} = -\frac{\omega r}{A_{in}}[\cos 2\varphi - \cos 2\alpha], \quad v_\varphi^{in} = \frac{\omega r}{A_{in}}[\sin 2\varphi - 2\varphi\cos 2\alpha]. \quad (6)$$

On the plates at $\varphi = \pm\alpha$, the boundary conditions are satisfied, *i.e.* $v_r^{in}(r, \pm\alpha) = 0, \quad v_\varphi^{in}(r, \pm\alpha) = \pm\omega r$. The solution in the outer region has an analogous form. The streamlines (isolines of ψ) are depicted in Figs S13 (a-d) for four different openings, $\alpha = 85.7°, 60°, 30°$ and $18°$. The corresponding vector velocity field is shown for illustration in Fig S13 (a). Note that the inner and outer solutions in Equation (6) are singular at $\varphi \cong 129°$ and $51°$, respectively. This singularity is probably a consequence of nonphysical geometry as infinite plate result in two disconnected semi-infinite fluid domains. Considering finite plates should regularize the solution, however, the closed-form solution in such case is not readily available. Nevertheless, the infinite plate approximation should provide an accurate description of the flow far from the plates' ends at with for $\alpha < 50°$.

The components of the rate-of-strain tensor, D_{ij}, for the inner region can be found from Equations (6) as

$$D_{rr}^{in} = \frac{\partial v_r^{in}}{\partial r} = -\omega A_{in}^{-1}[\cos 2\varphi - \cos 2\alpha],$$

$$D_{\varphi\varphi}^{in} = \frac{1}{r}\left(\frac{\partial v_\varphi^{in}}{\partial \varphi} + v_r^{in}\right) = \omega A_{in}^{-1}[\cos 2\varphi - \cos 2\alpha] = -D_{rr}^{in},$$

$$2D_{r\varphi}^{in} = \frac{1}{r}\left(\frac{\partial v_r^{in}}{\partial \varphi} - v_\varphi^{in}\right) + \frac{\partial v_\varphi^{in}}{\partial r} = 2\omega A_{in}^{-1} \sin 2\varphi.$$

Next we calculate the (squared) *rate-of-strain* $\Gamma^2 = \frac{1}{2} D_{ij} D_{ij}$ (the share rate $\dot{\gamma}$ is defined as $\dot{\gamma} = 2\Gamma$),

$$\Gamma^2 = \tfrac{1}{2} D_{rr}^2 + \tfrac{1}{2} D_{\varphi\varphi}^2 + D_{r\varphi}^2 = \omega^2 A_{in}^{-2}[1 - 2\cos 2\varphi \cos 2\alpha + \cos^2 2\alpha]. \quad (7)$$

The result in Equation (7) holds for the outer region with A_{in} being replaced with A_o. Note that for an infinite scallop Γ is not a function of r and depends solely on φ *i.e.* for an arbitrary opening Γ has a constant (but not equal!) values along the plates inside and outside.

The corresponding plots of Γ/ω are given in Fig S14(a-d) for the same four openings α as in Fig S13. This figure illustrates the underlying physics of the phenomenon, *i.e.*, the plates play a role of the *concentrator* of the strain rate. Similarly to the electric capacitor concentrating the energy of the electric field in between two oppositely charged plates, the flapping plates concentrate the strain rate of the liquid sandwiched between the plates at small α's. For Newtonian liquids this phenomenon is not important as both swimming and pumping are purely geometric, *i.e.* independent of time parameterization. Indeed, the fluid viscosity μ does not depend on the strain rate and remains constant so that over a full stroke such "scallop" would neither pump nor swim. For the non-Newtonian liquid, however, this phenomenon determines the essence of the effect. Since the apparent fluid viscosity μ_{app} is a function of the strain rate Γ, then the "scallop" modulates the viscosity of the suspending medium depending on contrast of the opening/closing frequencies. For shear thickening liquids the viscosity in the inner region could be considerably higher than that outside (compare Γ in Fig S14 (c)-(d) inside vs. outside). The dependence of the apparent viscosity on the strain rate distinguishes the liquid inside and outside the shells and results eventually in the free swimmer's locomotion or net momentum flux for a tethered pump.

To understand the origin of the motility heuristically (*vs.* arguments based on duality relation in the main text), consider the fundamental solution for the low-*Re* flow driven by a point force of magnitude $\boldsymbol{F}_p\delta(\boldsymbol{x})$ exerted on the fluid at the origin (this solution is known as *Stokeslet* [4]). One can argue that far from the object the origin of the force is not important – it equally can be submerged jet or flapping tethered "scallop". The properties of the source enters the solution integrally as a net momentum flux of magnitude F_p. If now the "scallop" becomes untethered, it will start moving with the characteristic speed, $V_s \sim F_p/\mu_0$. The crucial property of the swimmer is that it is propelled in the 'outer' liquid with low (approx. constant) viscosity μ_0, as in the outer region Γ is always small, see Fig S14 (a)-(d), whereas the viscosity of the fluid sandwiched between the two plates $\bar{\mu}_{\mathrm{app}}$ scales with the angular velocity of the *fast* (either closing or opening) stroke. The value of this internal viscosity determines the 'power' F_p of the source, $F_p \sim \bar{\mu}_{\mathrm{app}}\omega$, whereas major contribution to $\bar{\mu}_{\mathrm{app}}$ occurs at small opening α during the fast phase. Thus, the swimmer velocity V_s reduces to $V_s/\omega l \sim \bar{\mu}_{\mathrm{app}}/\mu_0$. This relation is in agreement with the estimate based on scaling arguments in the main text. The finite net displacement over a full stroke is due to modulation of the source strength, F_p, which depends on angular velocity ω in a nonlinear fashion via $\bar{\mu}_{\mathrm{app}}(\omega)$.

Hysteresis of viscosity in shear thickening liquids

To understand the difference in the experimentally measured pre-factors β we re-write the power-law rheological model at low- and intermediate shear rates $\dot{\gamma}$ as

$$\mu_{app} \approx 0.7\left(\frac{\dot{\gamma}}{\dot{\gamma}_c}\right)^{-0.1}, \quad 0.1\ \mathrm{s}^{-1} \leq \dot{\gamma} \leq 1.5\ \mathrm{s}^{-1},$$

$$\mu_{app} \approx 0.8\left(\frac{\dot{\gamma}}{\dot{\gamma}_c}\right)^{2.34}, \quad 1.5\ \mathrm{s}^{-1} \leq \dot{\gamma} \leq 6.5\ \mathrm{s}^{-1},$$

where $\dot{\gamma}_c = 1.5\ \mathrm{s}^{-1}$ is the *critical shear rate at steady conditions* [5].

It has been found first in [5], then in [5, 6, 7] that the transition taking place at at $\dot{\gamma} = \dot{\gamma}_c$ possesses the properties of the phase transition of the first order. Namely, the transition is characterized by the *hysteresis of viscosity upon varying the shear rate*. In particular, in experiment with transient shear rate the value of viscosity depends on the prehistory of shear rate ramp: if the shear rate grows *from a low viscosity state* the transition occurs at a higher critical shear

rate than in steady state ($\dot{\gamma} > \dot{\gamma}_c$). Analogously, if the shear rate decreases *from a high viscosity state*, the transition takes place at a lower values of transient shear rate comparing to the steady state ($\dot{\gamma} < \dot{\gamma}_c$) [5].

The hysteresis of viscosity explains the asymmetry in propulsion upon exchanging between (fast) closing and opening strokes. Since opening and closing strokes are not identical (at opening the angle between plates changes from 10° up to 295° they are different in the interval of 10°-65° For (fast) opening, the shear rate decreases from a high viscosity state, and for the (fast) closing cycle the shear rate increases. In agreement with the hysteresis described in [5] the "scallop" propelled by (fast) opening stroke swims better than the one than relies on (fast) closing stroke.

It has been found in [5, 6, 7] that the transition taking place at $\dot{\gamma} = \dot{\gamma}_c$ possesses the properties of the phase transition of the first order. Namely, the transition is characterized by the hysteresis of viscosity upon varying the shear rate. In particular, in experiment with transient shear rate the value of viscosity depends on the prehistory of shear rate ramp: if the shear rate increasesfrom a low viscosity state the transition occurs at a higher critical shear rate than in steady state ($\dot{\gamma} > \dot{\gamma}_c$). Analogously, if the shear rate decreases from a high viscosity state, the transition takes place at a lower values of transient shear rate comparing to the steady state ($\dot{\gamma} < \dot{\gamma}_c$) [5].The hysteresis of the shear thickening fluid was measured via a shear rate ramp loop test first from 1 s^{-1} up to 15 s^{-1} and then immediately from 15 s^{-1} down to 1 s^{-1}. The loop was repeated for three times and the average is plotted in Fig S10. In agreement with the previsous works, the transition occurs at a higher critical shear rate when the shear rate increases from a low viscosity (blue squares), and vice versa a lower critical shear rate when decreasing (red triangles).

This hysteresis explains the reason that the average displacement per cycle of the backward stroke is larger than that of the forward stroke, under the same ratio of closing and opening (the absolute value of pre-factor $\beta = -0.014$ in Fig 4(C) is larger than $\beta = 0.008$ in Fig 4(B)). Specifically, the closing and opening strokes of the macro-scallop are not identical: at closing, as the gap between the shells changes from large to small, the shear rate increases and thus the transition of shear thickening occurs at a higher critical shear rate; vice versa at opening, the gap increases, the shear rate decreases, and the critical shear rate is lower. Therefore, in the opening half-cycle, the swimmer exhibits higher average viscosity than that in the closing half-cycle, and consequently results in better propulsion.

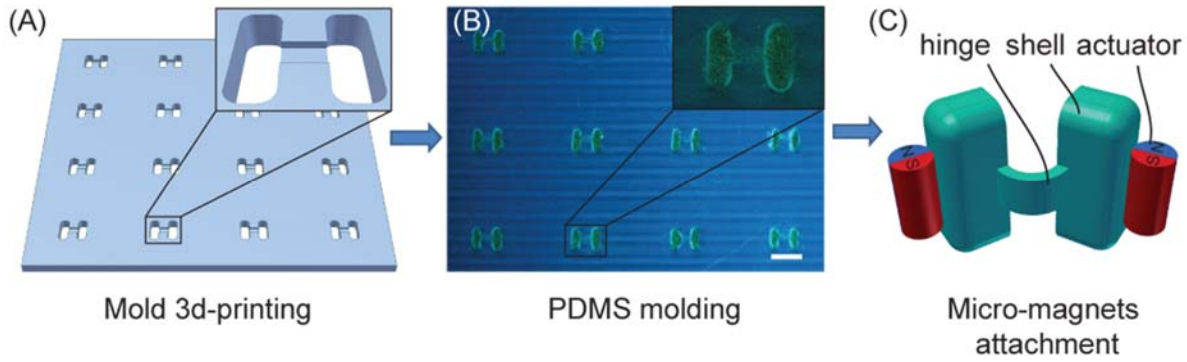

Fig S1. Fabrication process of the micro-scallop. (A) The negative mold of the micro-scallop is made by 3-D printing. The mold for the hinge is much shallower and narrower than the two shells. Shown in the inset is an enlargement of one mold. (B) As-printed molds filled with PDMS polymer containing green fluorescent powder imaged under UV light (scale bar is 1 mm). (C) 3-D model of the resultant micro-scallop. The PDMS part (green) is released after curing and two micro-magnets are attached in the orientation indicated in the schematic. A more detailed description of the fabrication procedure is illustrated in Fig S3.

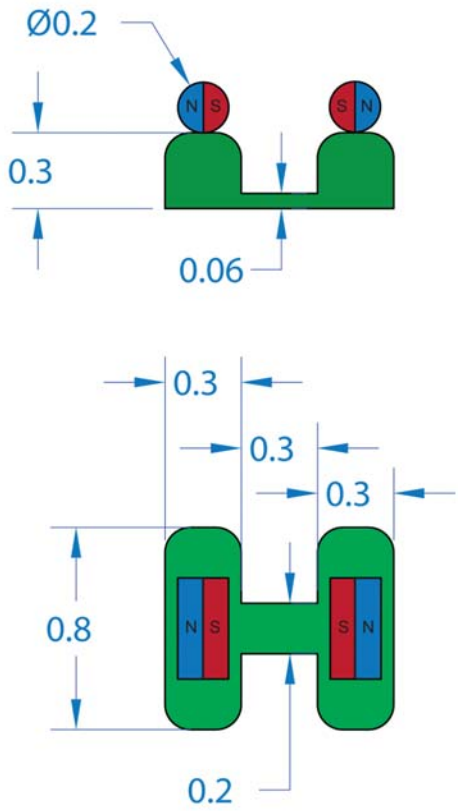

Fig S2. Detailed dimensions of the micro-scallop. Important dimensions of the micro-scallop are drawn in the figure in the unit of millimeter.

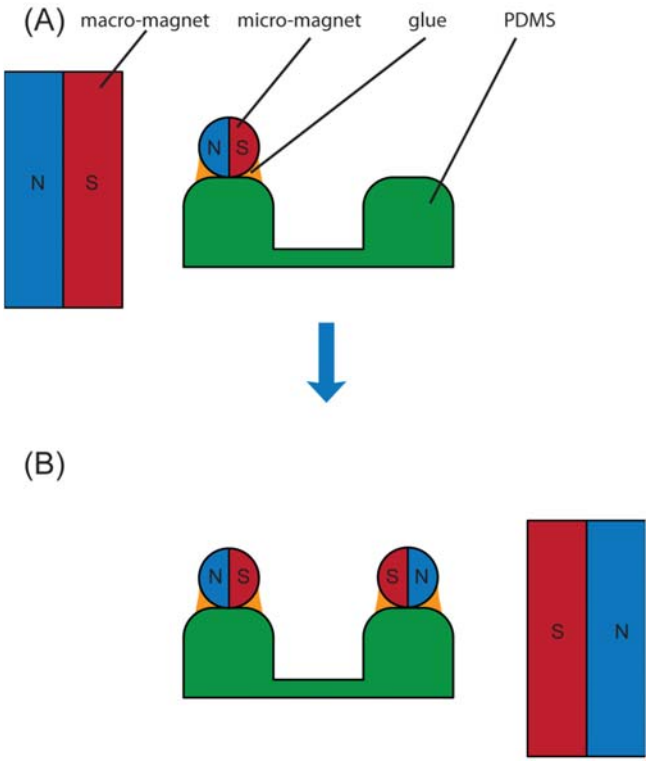

Fig S3. Illustration of the micro-magnets attachment process. (A) Step 1, the first micro-magnet (left) is attached to the PDMS by glue, while its orientation is kept by the macro-magnet. (B) Step 2, after the fixation of the first magnet, the second micro-magnet (right) is attached to the PDMS by glue. The local field is dominated by the macro-magnet on the right, so the orientation of the second micro-magnet is kept in the opposite direction of the first. The macro-magnet is not drawn to scale.

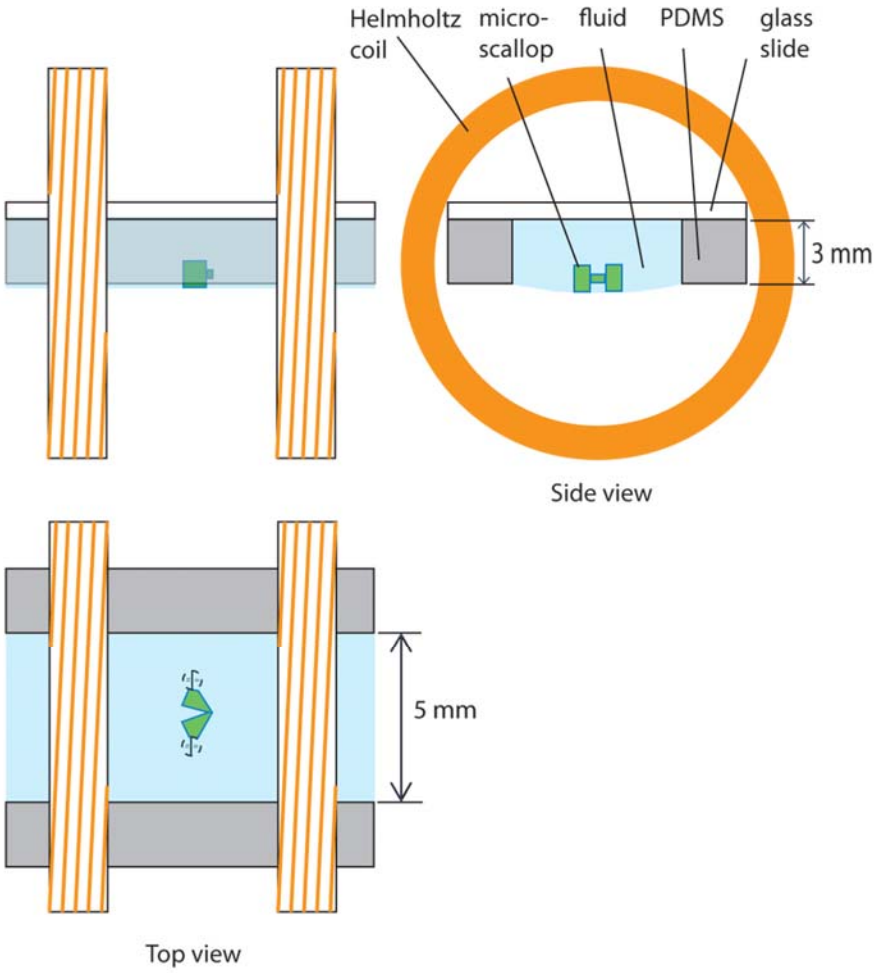

Fig S4. The actuation setup for the micro-scallop. The micro-scallop is not drawn to scale.

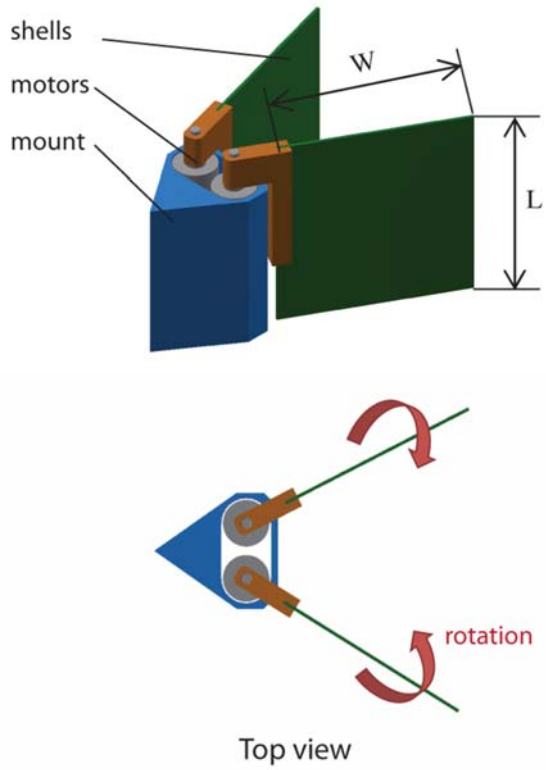

Fig S5. Macro-scallop 3-D model and its top view illustrating the closing motion of the two shells.

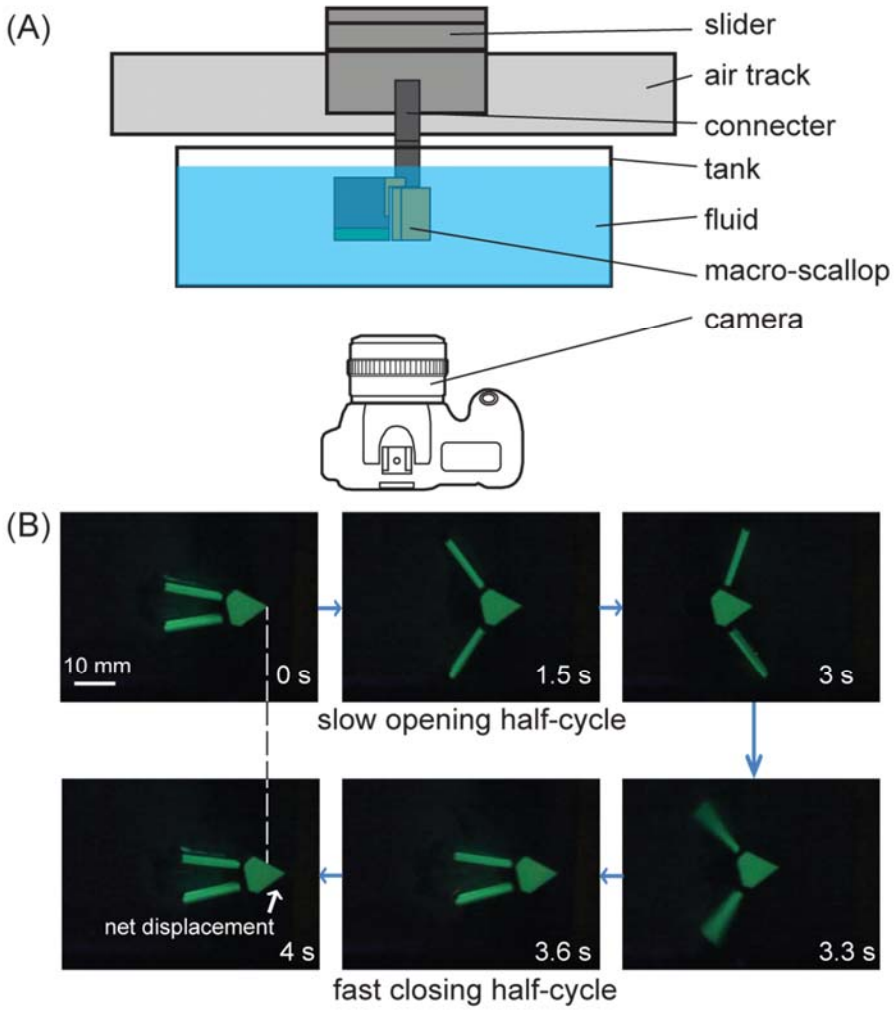

Fig S6. Propulsion experiments of the macro-scallop. (A) An illustration of the experimental setup for the macro-scallop. (B) Time-lapse pictures of asymmetric actuation of the macro-scallop in shear thickening fluid. The three pictures in the first line correspond to the slow opening half-cycle (~3 s) and the pictures in the second line correspond to the fast closing half-cycle (<1 s). The net displacement is observed by comparing the pictures at 0 s and 4 s with the dashed line aligned with the tip of the macro-scallop at 0 s.

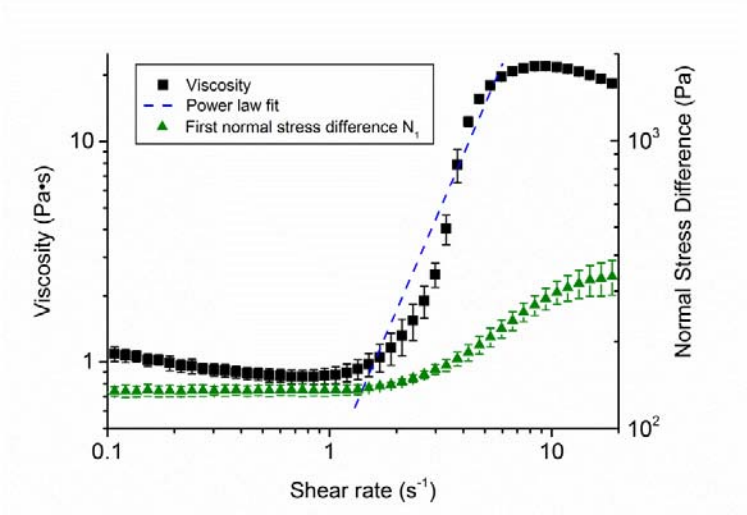

Fig S7. Apparent dynamic viscosity of the shear thickening fluid. Power law model (dotted line) is used to fit the viscosity (black squares) in the shear rate range of 1.5~6 s^{-1}. The change of first normal stress difference N_1 of our shear thickening medium is two orders of magnitude smaller than the Boger fluid used in [8]. Thus, the viscosity change is dominant during the swimming process. The error bars represent standard deviations.

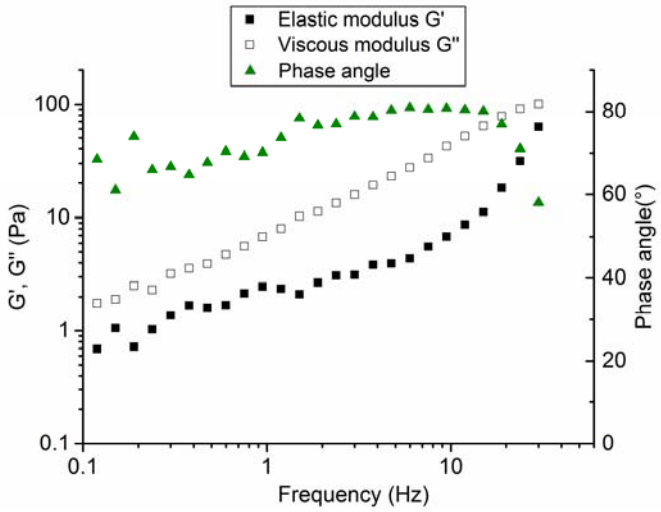

Fig S8. Oscillation test of the shear thickening fluid. The viscous modulus G'' is more than 2 times larger than the elastic modulus G' over the frequency range of 0.1~20 Hz, and the phase angle is 70º ~80º, which both indicate that the viscosity is dominant over elasticity for the shear thickening fluid.

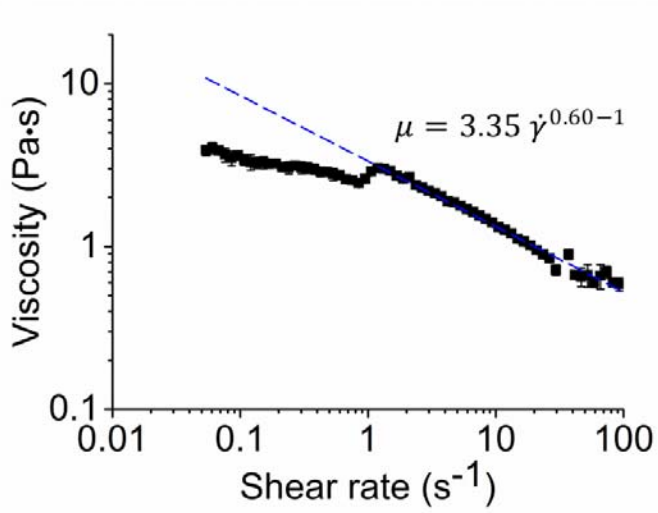

Fig S9. Apparent dynamic viscosity of the shear thinning fluid. Power law model (dotted line) is used to fit the data in the shear rate range of 1~100 s^{-1}. The error bars represent standard deviations.

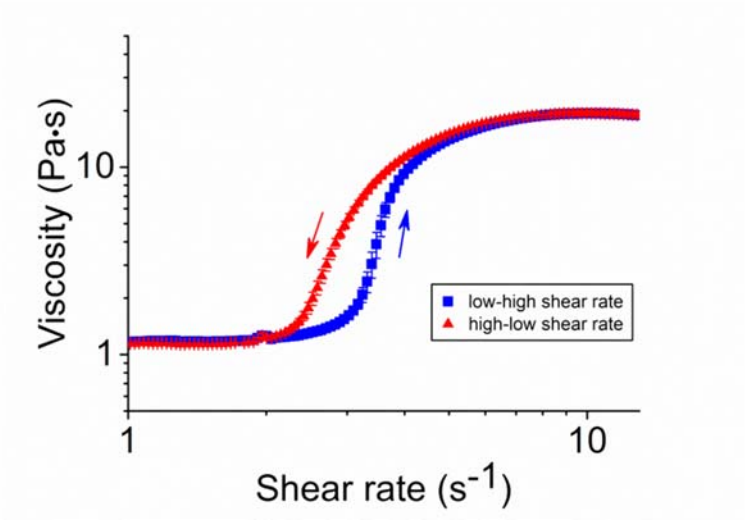

Fig S10. Hysteresis of viscosity of the shear thickening fluid. When the shear rate increases from a low viscosity (blue squares), the transition occurs at a higher critical shear rate, while when the shear rate decreases from a high viscosity (red triangles), the transition takes place at a lower shear rate. The error bars represent standard deviations.

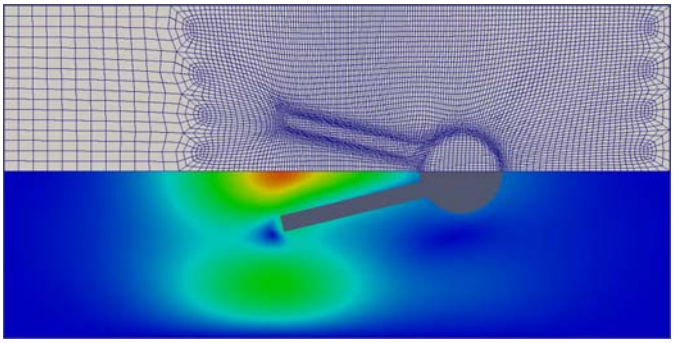

Fig S11. The vertices of the computational mesh are concentrated near the surface of the macro-scallop to improve resolution of the liquid-solid interface. The color in the lower half shows the velocity field of the fluid.

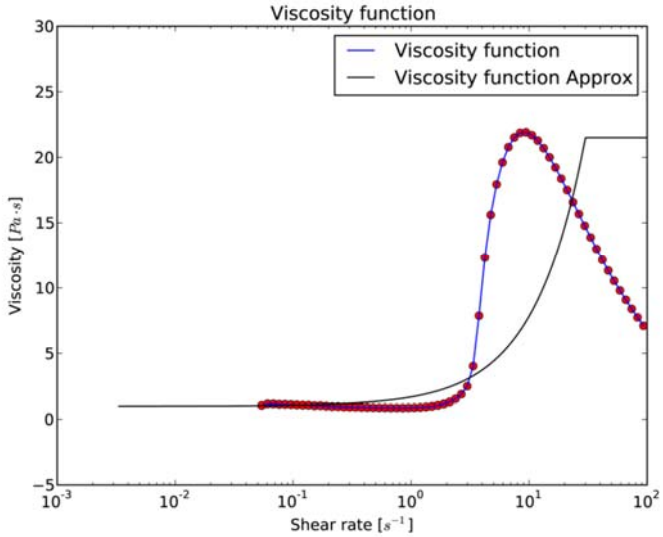

Fig S12. Approximation of the viscosity for shear thickening fluid for convergence in numerical simulation. Red circles are measured data points in experiment, blue line is the trend line, and the black line is the approximation used in numerical simulation.

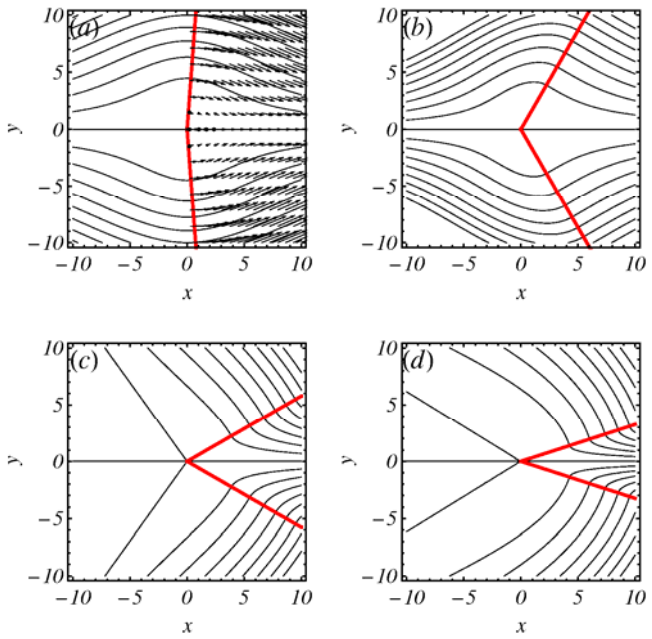

Fig S13. Flow pattern (streamlines) due to a 2D tethered infinite "scallop" (pump) upon varying the opening $\boldsymbol{\alpha}$=85.7°(*a*), 60°(*b*), 30°(*c*) and 18°(*d*); position of the plates are marked by thick red lines. The corresponding vector velocity field is in (*a*) for the closing stroke.

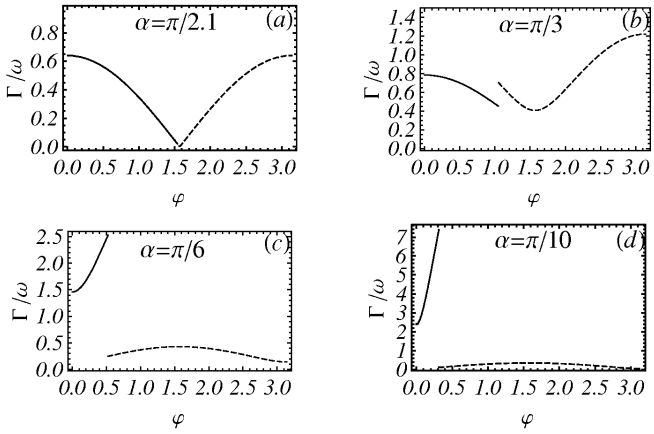

Fig S14. The scaled strain rate $\boldsymbol{\Gamma/\omega}$ for the 2D infinite tethered "scallop" (pump) *vs.* a polar angle $\boldsymbol{\varphi}$ for the same openings $\boldsymbol{\alpha}$ as in Fig S13 (shown in radians). Solid lines stand for the inner region and the dashed lines stand for the outer region.

List of Supplementary Movies

Supplementary Movie 1

Micro-scallop in shear thickening fluid. Net displacement in x direction was achieved by asymmetric actuation of slow-open-fast-close (upper panel), in comparison, no net displacement in x direction by symmetric actuation (lower panel). The movie was for 4-times speeded up.

Supplementary Movie 2

Micro-scallop in shear thinning fluid. Net displacement in x direction was achieved by asymmetric actuation of fast-open-slow-close (upper panel), in comparison, no net displacement in x direction by symmetric actuation (lower panel). The movie was for 4-times speeded up.

Supplementary Movie 3

Micro-scallop in Newtonian fluid. An asymmetric actuation of slow-open-fast-close was applied to the micro-scallop and no net displacement in x direction was observed. The movie was for 4-times speeded up.

Supplementary Movie 4

Numerical simulation results of the velocity fields around the macro-scallop under asymmetric slow-open-fast-close actuation. Upper panel: the swimmer in Newtonian fluid results in no net displacement; lower panel: the swimmer in shear thickening fluid results in net displacement.

Supplementary Movie 5

Numerical simulation shows the velocity (upper panel) and viscosity fields (lower panel) of the shear thickening fluid around the macro-scallop under asymmetric slow-open-fast-close actuation.

Supplementary Movie 6

Experimental video shows asymmetric slow-open-fast-close actuation of the macro-scallop resulted in net displacement in shear thickening fluid. The movie was for 2-times speeded up.

Supplementary Movie 7

Experimental video shows symmetric actuation of the macro-scallop resulted in no net displacement in shear thickening fluid. The movie was for 2-times speeded up.

Supplementary Movie 8

Experimental video shows asymmetric slow-open-fast-close actuation of the macro-scallop resulted in no net displacement in a Newtonian fluid. The movie was for 2-times speeded up.

References

1. Munster R, Mierka O, Turek S. Finite element-fictitious boundary methods (FEM-FBM) for 3D particulate flow. *Int J Numer Meth Fl* **69**, 294-313 (2012).
2. Normand T, Lauga E. Flapping motion and force generation in a viscoelastic fluid. *Phys Rev E* **78**, (2008).
3. Moffatt HK. Viscous and Resistive Eddies near a Sharp Corner. *Journal of Fluid Mechanics* **18**, 1-18 (1964).
4. Kim S, Karrila SJ. *Microhydrodynamics*. Butterworth-Heinemann (1991).
5. Laun HM, Bung R, Schmidt F. Rheology of Extremely Shear Thickening Polymer Dispersions (Passively Viscosity Switching Fluids). *J Rheol* **35**, 999-1034 (1991).
6. Nakanishi H, Nagahiro S, Mitarai N. Fluid dynamics of dilatant fluids. *Phys Rev E* **85**, 011401 (2012).
7. Deegan RD. Stress hysteresis as the cause of persistent holes in particulate suspensions. *Phys Rev E* **81**, 036319 (2010).
8. Keim NC, Garcia M, Arratia PE. Fluid elasticity can enable propulsion at low Reynolds number. *Phys Fluids* **24**, 081703 (2012).